Limnol. Oceanogr., 58(2), 2013, 489–504
© 2013, by the Association for the Sciences of Limnology and Oceanography, Inc.
doi:10.4319/lo.2013.58.2.0489

Spectral irradiance dependence of sunlight effects on plankton dimethylsulfide production

Martí Galí,* Clara Ruiz-González, Thomas Lefort, Josep M. Gasol, Clara Cardelús, Cristina Romera-Castillo, and Rafel Simó

Institut de Ciències del Mar (CSIC), Barcelona, Catalonia, Spain

Abstract

We investigated the short-term effects of variable solar irradiance and spectrum on the gross biological production of dimethylsulfide (DMS), a trace gas with potential climatic effects, in eight experiments performed at different times of the year in a northwest Mediterranean coastal site. Experimentally determined net community DMS production, DMS photolysis, and dark microbial DMS consumption rates were used to calculate gross community DMS production by budgeting. In addition, the composition of the bacterioplankton and phytoplankton communities in the initial samples, and the photoinhibition of bulk bacterial heterotrophic activity and phytoplankton photosynthetic efficiency were monitored. Our results show that: (1) gross DMS production is irradiance dependent, with a maximum short-term stimulation factor of 2- to 6-fold compared to dark incubations; (2) its spectral shape is variable but generally similar to that of phytoplankton photoinhibition or photodamage, with more effective stimulation at shorter ultraviolet wavelengths; and (3) stronger stimulation occurs when samples are overexposed with respect to their prior exposure. Remarkably, the photoresponse of gross DMS production was in most cases strong enough to (at least) compensate the photochemical DMS loss at the water subsurface. Such response would prevent DMS depletion in stratified and highly irradiated waters. Since the initial microbial communities were representative of meso- to oligotrophic conditions, our observations should apply to a wide variety of oceanic regimes.

Solar radiation is a major driver of biogeochemical processes. In recent decades, our understanding of how the ultraviolet (UV; 280–400 nm) region of the spectrum influences major carbon and nutrient cycling pathways (e.g., photosynthesis, heterotrophic activity, and photochemical reactions), as well as its effects on organism survival and population dynamics, has increased significantly (Sommaruga 2003; Zepp et al. 2007). In parallel, spectrally resolved models for photochemical and photobiological processes have been developed (Neale and Kieber 2000). Despite all these facts, routine measurements of biogeochemical processes naturally occurring under sunlight are seldom conducted under UV radiation (UVR)–inclusive conditions.

Dimethylsulfide (DMS) is a volatile sulfur compound produced at the ocean's surface as a result of microbial cycling of dimethylsulfoniopropionate (DMSP), an ubiquitous algal osmolyte (Simó 2004). The oceanic emission of this single volatile annually transfers ~ 28 Tg of sulfur to the atmosphere (Lana et al. 2011), and some of it back to land, balancing biospheric sulfur budgets. Atmospheric DMS oxidation influences aerosol chemistry, potentially promoting the formation of cloud condensation nuclei in remote marine regions. Twenty-five years ago, a paradigm-changing paper (Charlson et al. 1987) proposed that, if DMS emission resulted in increased cloud albedo and, in turn, it responded positively to irradiance or temperature, a negative feedback would operate between oceanic plankton and the earth's radiative budget. Since the so-called CLAW hypothesis (after the author's initials) was postulated, several studies have unveiled the complexity of oceanic DMS cycling (Simó 2004; Stefels et al. 2007) and, although the feasibility of the whole hypothesis remains controversial (Quinn and Bates 2011), there is a growing body of evidence pointing at solar radiation as a major driver of DMS cycling (Simó 2004; Vallina and Simó 2007; Lana et al. 2012).

DMSP is a multifunctional zwitterion found at high concentrations in the cytosol of various phytoplankton groups, mainly prymnesiophytes, dinoflagellates, chrysophytes, prasinophytes, and pelagophytes (Stefels et al. 2007). Some algal DMSP producers can enzymatically cleave it to DMS (and acrylate), but the cleavage activity varies widely within phytoplankton groups and even among different strains of the same ''species.'' In addition, a major portion of algal DMSP is released to the dissolved phase due to algal exudation, senescence or autolysis, viral lysis, and microzooplankton grazing (Stefels et al. 2007). Dissolved DMSP (DMSPd) undergoes active microbial cycling (Vila-Costa et al. 2006; Moran et al. 2012), but only a minor fraction of microbially consumed DMSP results in DMS production by bacterial enzymes, the remainder being diverted into microbial biomass and nonvolatile compounds (Kiene and Linn 2000; Moran et al. 2012). In turn, seawater DMS is readily oxidized, either by bacteria or by photochemical reactions, and only a minor fraction is vented to the atmosphere (Simó 2004; Stefels et al. 2007; Vila-Costa et al. 2008).

Several processes in this dimethylated sulfur cycling scheme are influenced by sunlight. At the global scale, this seems to translate into a strong correlation between average irradiance in the upper mixed layer and DMS concentrations (Vallina and Simó 2007; Lana et al. 2012). Algal

* Corresponding author: marti.gali.tapias@gmail.com

DMSP synthesis has been interpreted as a physiological adaptation to high light and nutrient limitation. Stefels (2000) suggested that DMS(P) excretion could constitute an overflow mechanism for excess reduced compounds when phytoplankton undergo unbalanced growth. Shortly thereafter, Sunda et al. (2002) put forward the antioxidant hypothesis, whereby intracellular DMSP cleavage would allow the scavenging of reactive oxygen species by DMS, acrylate, and subsequent DMS oxidation products (dimethylsulfoxide and methanesulfinic acid). At the ecosystem level, sunlight modulates microbial DMSPd utilization (Slezak et al. 2007), and the relative importance of heterotrophic and autotrophic DMSPd consumers (Ruiz-González et al. 2012*b*). On the other hand, DMS sinks are also related to sunlight: UVR inhibits bacterial DMS consumption (Toole et al. 2006; Kieber et al. 2007) and drives DMS photolysis (Toole et al. 2003).

Recently, Galí et al. (2011) reported that gross DMS production was stimulated by the exposure to full-spectrum sunlight, in water samples from distinct coastal and open-ocean ecosystems. However, several uncertainties remained regarding the irradiance response patterns, the specific regions of the solar spectrum promoting such response, and the interplay between solar exposure and microbial community structure and activity. In the present work we have addressed these issues by means of eight short incubation experiments, combining bulk DMS cycling budgets with an array of algal and bacterial physiological indicators. Our results improve the current understanding of ecosystem gross DMS production, which is, despite its importance, a poorly constrained term in models of dimethylated sulfur cycling.

Methods

Sampling and experimental setting—Between summer 2008 and winter 2010, surface-water samples (0.5 m depth) were collected on eight occasions at the Blanes Bay Microbial Observatory (BBMO), a northwest Mediterranean coastal site (< 24 m depth; ~ 800 m offshore; 41°39.9′N, 2°48.3′E). BBMO is well characterized in terms of bacterioplankton and phytoplankton community succession (Alonso-Sáez et al. 2008; Gutiérrez-Rodríguez et al. 2011) and dimethylated sulfur cycling (Vila-Costa et al. 2008; Simó et al. 2009). One experiment was conducted in late winter (WI1), three in spring (SP1, SP2, and SP3) and summer (SU1, SU2, and SU3), and one in early autumn (AU1), covering the phytoplankton succession from bloom to low-biomass conditions (Table 1).

The samples were taken before sunrise to avoid prior exposure to sunlight, and brought within 2 h to the laboratory in dimmed polycarbonate carboys. In situ temperature and salinity profiles were measured with a conductivity–temperature–depth (CTD) probe (SAIV A/S model SD204) also equipped with turbidity and chlorophyll *a* (Chl *a*) fluorescence sensors. Underwater UVR and photosynthetically active radiation (PAR) profiles could not be measured on experiment days as we sampled before sunrise. Instead, radiation profiles obtained in the routine monthly sampling at BBMO (since 2008) were used to

Table 1. Summary of the water column conditions on the sampling dates, and initial sample characteristics. Temp. is the temperature. MLD stands for mixed layer depth. $K_{d,320}$ is the diffuse attenuation coefficient for 320 nm wavelength radiation (WI, winter; SP, spring; SU, summer; and AU, autumn).

Experiment	Date	Temp. (°C)	Salinity	MLD (m)	$K_{d,320}$ (m^{-1})	Chl *a* ($\mu g\ L^{-1}$)	Chl $a < 3\ \mu m$ ($\mu g\ L^{-1}$)	Bacteria (10^5 cells mL^{-1})	DMS (nmol L^{-1})	DMSPt (nmol L^{-1})
WI1	18 Mar 2010	11.9	37.7	15	0.44	1.25	0.42	8.5	3.2	6.8
SP1	12 May 2009	15.2	37.8	9	0.37	0.54	0.27	6.9	3.1	46.3
SP2	26 May 2009	16.8	37.6	8	0.34	0.58	0.27	8.9	6.2	38.5
SP3	09 Jun 2009	16.5	38.0	8	0.32	0.30	0.13	12.3	3.3	14.6
SU1	09 Jul 2008	23.0	37.8	4	0.35	0.20	0.15	8.5	9.0	48.6
SU2	30 Jun 2009	17.8	38.2	6	0.28	0.12	0.06	8.8	3.6	13.2
SU3	21 Jul 2009	20.3	38.1	8	0.26	0.13	0.03	9.4	3.4	15.9
AU1	30 Sep 2008	20.2	38.3	4	0.34	0.23	0.14	7.5	1.3	18.6

Table 2. Summary of experimental manipulations and their corresponding treatment code (*see* text for a detailed description). The irradiance transmitted by each bottle type in different wavebands is also given (*see* Fig. 2). Bio., biological. D, dark treatment.

		Transmitted irradiance (%)				Mean duration	
Treatment	Bottle material	UVB	UVA	PAR	Neutral screens (No.)	Bio. processes	Photolysis
T	Teflon	65	77	100	0–1	5.7	3.8
T_{dim}					1–3	7.1	4.2
PC	Polycarbonate	11	77	100	0–1	6.7	3.8
PC_{dim}					1–3	7.6	4.2
D	Glass (dark)	0	0	0		8.7	5

reconstruct the underwater radiation field, in conjunction with CTD and meteorological data (*see* below).

A gradient of spectral irradiance was created by manipulating total irradiance and the UV region of the spectrum, making a total of five treatments: two spectral treatments, with two irradiance levels each, plus one dark treatment (Table 2). Total irradiance was regulated using a variable number of neutral screen layers, adjusted in each experiment to match in situ mixing conditions. Spectral manipulation was achieved using incubation bottles with different spectral transmittance: polytetrafluoroethylene bottles (Teflon®, Nalgene; abbreviated T), which transmit the full solar spectrum, and polycarbonate bottles (Nalgene; abbreviated PC), which have the 50% cutoff at 339 nm, eliminating almost all ultraviolet B radiation (UVB; 280–320 nm). Thus, the high-irradiance treatments (T and PC) had their dimmed counterparts (labeled T_{dim} and PC_{dim}). Biological DMS cycling rates were measured in whole water samples, incubated in single or duplicate 2.3 liter bottles. DMS photolysis was measured in duplicate or triplicate bottles (40–250 mL), filled with 0.22 μm filtered water obtained from a sequential filtration system connected to a peristaltic pump (system routinely used for DNA collection, with 3 and 0.22 μm pore-size filtration cartridges). Biotic and abiotic process bottles, covered by $\sim$ 5 cm of running seawater, were incubated in a black tank on the roof of the lab. Spectral irradiance at the water subsurface was continuously recorded with a profiling UV (PUV-2500, Biospherical) multichannel radiometer placed inside the tank.

The experiment work flow was as follows: when the carboy arrived at the lab, aliquots for the determination of initial parameters were withdrawn, and the black plastic bag that covered the carboy was removed to allow some degree of initial photoacclimation in room light. The biological process bottles were filled without bubbling, after gently mixing the carboy, using silicone tubing. All the materials used were cleaned with hydrochloric acid, Milli-Q water, and the same seawater sample. Once all biological process bottles had been filled (within 30 min), they were immediately set in the incubation tank ($\sim$ 3 h before solar noon). DMS photolysis incubations started around 1 h after whole water incubations, and were stopped after 3–4 h of exposure. Biological process incubations lasted for 5–9 h, after which aliquots were taken to measure DMS and total DMSP (DMSPt), postexposure bacterial heterotrophic activity, and the photosynthetic performance of phytoplankton (*see* below).

Sample processing and analysis—DMS and DMSP analysis: DMS and DMSP were analyzed using a purge-and-trap system coupled to sulfur-specific gas chromatography (Shimadzu GC14A) with flame photometric detection. For DMS analysis (analyzed $<$ 1 h after the end of the incubation) 3–5 mL of seawater were gently passed through a syringe filter (GF/F, Whatman) and immediately sparged in a crimp glass vial for 3–5 min with 40 mL min^{-1} of high-purity helium (He). Volatiles were trapped in a 3.175 mm Teflon tube loop submerged in liquid nitrogen, from where they were revolatilized by dipping the loop in hot water. Sulfur compounds were separated using a packed Carbopack® 60/80 mesh column (Sigma-Aldrich) maintained at 170°C. Retention time for DMS was 0.9 min, and detection limit was 3 pmol. Analytical precision was better than 5%. Calibration was performed by syringe injection into the purge vial of varying volumes of a gaseous mixture of He and DMS released by a weight-calibrated permeation tube (Dynacal, Valco Instruments Co. Inc.) (Simó 1998). Plots of log(nmol DMS) vs. log(peak area) yielded a straight line (usually $R^2 > 0.99$) that was used for DMS quantification in the samples. For DMSPt analysis, a larger volume of unfiltered sample (40 mL) was stored in crimp glass vials after adding two NaOH pellets (45 mg each, $\sim$ 0.2 mol L^{-1} final concentration, pH $>$ 12). The DMSPt + DMS pool was analyzed as evolved DMS after undergoing alkaline hydrolysis for at least 24 h (and always within 2 weeks). The DMSPt concentration was calculated by subtraction of the previously determined DMS concentration.

Other chemical analyses: Dissolved inorganic nutrients (only nitrate + nitrite are reported here) were analyzed in an Alliance Evolution II autoanalyzer with spectrophotometric detection. For Chl *a* analysis, 150 mL of seawater was filtered through GF/F filters (Whatman), extracted in acetone (90% v:v, 4°C, overnight), and measured in a Turner Designs fluorometer. Picoplankton Chl *a* was determined by parallel filtration onto GF/F after screening with polycarbonate 3 μm pore filters (Poretics). Samples for colored (or chromoporic) dissolved organic matter (CDOM) were measured immediately after filtration following Romera-Castillo et al. (2012). Seawater was filtered by an acid-cleaned glass filtration system using precombusted GF/F filters. CDOM absorption was measured in a dual-beam spectrophotometer (Varian Cary 100 Bio) equipped with a 10 cm quartz cell. Spectral scans were collected between 250 and 750 nm at a constant room temperature of 20°C. Milli-Q water was used as blank.

Absorption coefficients of CDOM were calculated as $a_{CDOM,\lambda} = 2.303\ Abs_\lambda\ R^{-1}$, where Abs_λ stands for absorbance at wavelength λ, and R for the optical path length in meters (0.1 m cuvette). The spectral slope of CDOM (S_{CDOM}) was computed from the linear regression between the natural logarithm of $a_{CDOM,\lambda}$ and wavelength at the range 300–400 nm.

Phytoplankton counts and carbon biomass: Picocyanobacteria (*Prochloroccus* and *Synechococcus*) and picoeukaryotic phytoplankton populations were enumerated in live samples by flow cytometry (FACScalibur, Beckton Dickinson) (Marie and Partensky 2006). Autotrophic nanoplankton (nanoflagellates and cryptophytes) were counted using epifluorescence microscopy in samples stained with 4,6-diamidino-2-phenylindole (DAPI). Microphytoplankton species (dinoflagellates and diatoms) were identified and counted with an inverted microscope in samples preserved with formalin-hexamine (0.4% final concentration) and kept at 4°C. Carbon biomass was estimated using standard conversion factors for picophytoplankton (following Simó et al. 2009), or factors based on cell size for nano- and microphytoplankton (Menden-Deuer and Lessard 2000).

Phytoplankton photosynthetic efficiency: Maximum quantum efficiency of photosystem II photochemistry ($F_v : F_m$) was measured using a Fast Repetition Rate fluorometer (FRRf; Fasttracka, Chelsea Marine Systems), and interpreted as a proxy for photoinhibition and photodamage. Subsamples of 60 mL were withdrawn from the incubation bottles and allowed to recover from short-term photoinhibition during 5 min in dim light, and subsequently placed in the dark chamber of the FRRf. The protocol consisted of 100 saturation flashlets (1.3 μs duration, 2.8 μs interflash delay) followed by 20 relaxation flashlets (separated by 50 μs). Thirty acquisitions were averaged for each sample, and the resulting saturation curve was fitted using the version 5 (v5) Matlab software (Laney 2003), which allows correcting for 0.2 μm filtered water blanks and for the instrument's response function. All samples were analyzed in duplicate. When needed, additional bottles were set in the incubator to measure $F_v : F_m$ at intermediate time points.

Particulate primary production (PPp): Photosynthesis–irradiance curves were measured on the initial water samples and used to estimate PPp in each experimental treatment. Thirteen 70 mL bottles (Corning) and one dark control were filled with seawater and inoculated with 10 μCi $NaH^{14}CO_3$. The incubation was carried out in a water bath at in situ temperature in a gradient of artificial PAR (10–1000 μmol photons $m^{-2}\ h^{-1}$). After 2 h of incubation the samples were filtered at low vacuum through cellulose ester filters (Millipore 0.22 μm), which were subsequently exposed overnight to concentrated HCl fumes. Scintillation cocktail (4 mL Optiphase Hisafe 2) was then added to each filter, and the radioactivity was measured in a Beckman LS6000 scintillation counter. The photosynthesis–irradiance curves showed no photoinhibition at high PAR, so they were fitted using the model of Webb et al. (1974). Uninhibited photosynthesis rates in the incubations were calculated at 1 min resolution using the photosynthesis–irradiance curve–derived parameters (P^b_{max} and α) and the PAR measured in the tank. UVR-inhibited PPp rates were recalculated by multiplying, at each time step, uninhibited PPp by the relative inhibition of $F_v : F_m$ (interpolated at 1 min resolution). The rates were finally averaged over the duration of the experiment.

Bacteria counts: Samples were fixed with 1% paraformaldehyde + 0.05% glutaraldehyde (final concentration), flash-frozen in liquid nitrogen, and stored at −80°C. Bacterial populations were enumerated with a FACSCalibur flow cytometer (Becton Dickinson) following standard procedures (Gasol and del Giorgio 2000).

Catalyzed reporter deposition–fluorescence in situ hybridization (CARD-FISH): Hybridization with phylogenetic probes targeting major bacterial groups allowed the determination of the bacterial community composition in the initial sample. The clades targeted were *Gammaproteobacteria*, NOR5 (within *Gammaproteobacteria*), *Bacteroidetes*, *Roseobacter*, SAR11 (the last two, members of *Alphaproteobacteria*), and *Synechococcus*, as well as *Eubacteria*. Counterstaining of CARD-FISH filters was done with DAPI. We used the protocol of Pernthaler et al. (2002). Further details can be found in Ruiz-González et al. (2012*a*).

Bulk bacterial heterotrophic activity: Initial and postexposure bacterial heterotrophic activities were estimated with the ^{3}H-leucine incorporation method (Kirchman et al. 1985) in triplicate samples (plus one killed control), processed by the centrifugation method of Smith and Azam (1992).

Optics and spectral weighting functions—In situ radiation field. The in situ exposure regime was calculated combining UVR and PAR attenuation profiles, mixing depths obtained from the CTD casts, and the spectral irradiance at the water subsurface recorded by the PUV-2500 placed in the incubator. Diffuse attenuation coefficients of downwelling cosine irradiance ($k_{d,\lambda}$) were calculated for each of the radiation bands measured by the PUV-2500 (six in the UV, centered at 305, 313, 320, 340, 380, and 395, and one single band in the PAR) assuming an exponential extinction (after discarding the first 2 m from the surface). In addition, k_d's for the UVB and ultraviolet A radiation (UVA; 320–400 nm) bands were calculated by spectrally integrating PUV-2500 profiles. Since we had no direct measurements on the date of sampling, each experiment was assigned the k_d's from the closest sampling, if the water column conditions were very similar. Otherwise, k_d's were calculated as function of Chl *a* and turbidity, which were good predictors of underwater light attenuation at this site (M. Galí et al. unpubl.). The mixed layer depth was calculated from both temperature and density (σ_t) profiles, binned at 1 m resolution, as the depth where either temperature or density departed > 0.15°C or kg m^{-3} from the surface reference value (2 m depth). For each radiation band, subsurface irradiance, vertically integrated irradiance in the mixed layer (Vallina and Simó 2007), and that at the bottom of the mixed layer were computed for the duration of each experiment (Fig. 1).

Experimental radiation field: The calibrated UVR time series recorded by the PUV-2500 in each experiment (six discrete bands) was spectrally interpolated with the shape of a standard, high-resolution non-calibrated spectrum. The standard spectrum was obtained by averaging several standardized spectra measured with a miniature diode array spectroradiometer (USB2000+, Ocean Optics) on sunny days around noon. Standardized spectra showed very little variation and were in good agreement with published ones (Gueymard et al. 2003). This way, an average UVR spectrum between 300 and 400 nm at the water subsurface, with 1 nm resolution, was produced for each experiment and treatment. The USB2000+ (equipped with a cosine detector) was also used to measure the spectral irradiance inside and outside the T and PC bottles to calculate their spectral transmittance (Fig. 2A). These measurements were corrected by transmittance measurements done with a scalar irradiance spherical PAR sensor, to better take into account the three-dimensional radiation field. Finally, the product of subsurface spectral irradiance, bottle transmittance, and neutral screen attenuation yielded the actual spectral irradiance ($E_{d,\lambda}$) experimented by the samples, which is the basis of further calculations.

Spectral weighting functions: UVR-mediated reactions have a strong spectral dependence. Therefore, $E_{d,\lambda}$ was weighted with spectral functions found in the literature. All weighting functions were normalized to 1 at 300 nm; thus, they were used as a dimensionless spectral efficiency. Spectral integration (or sum, in discrete form) of weighted $E_{d,\lambda}$ yielded the weighted UV irradiance E^*:

$$E^* = \sum_{\lambda=300\text{nm}}^{400\text{nm}} E_{d,\lambda}\varepsilon_\lambda \quad (1)$$

where ε_λ is a wavelength-dependent scaling coefficient. Since ε_λ has inverse energy units ($m^2\ W^{-1}$) in the photobiological literature but inverse quantum units (m^2 quanta^{-1} s^{-1}) in the photochemical literature, we converted $E_{d,\lambda}$ to quantum units, when necessary, using Planck's constant. E^* was converted to weighted irradiance dose (H^*) multiplying it by the duration of the exposure.

DMS photolysis: DMS photolysis can be described by apparent spectral quantum yields (ϕ_λ) that decrease exponentially with wavelength (Toole et al. 2003). An average ϕ_λ was produced by averaging four spectral slopes, obtained from two studies done at the Sargasso Sea and the Bering Sea (Toole et al. 2003; Deal et al. 2005). The resulting ϕ_λ had a spectral slope of 0.0436 nm^{-1} (with the original slopes ranging between 0.0321 and 0.0499). DMS photolysis is a photosensitized process, meaning that actinic light is not directly absorbed by DMS. Thus, ϕ_λ has to be multiplied by the amount of light absorbed by CDOM (Fig. 2B–D) to obtain the photolysis-weighted irradiance as

$$E^*_{\text{photo}} = \sum_{\lambda=300\text{nm}}^{400\text{nm}} E_{d,\lambda}a_{\text{CDOM},\lambda}\phi_\lambda \quad (2)$$

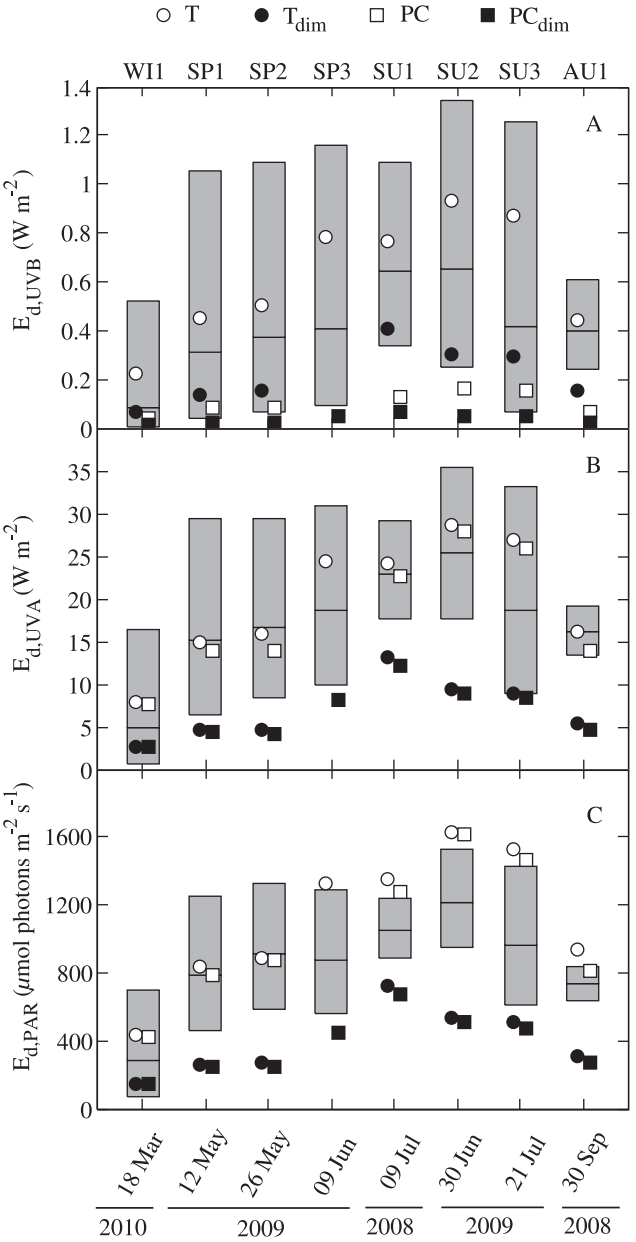

Fig. 1. Comparison between in-situ and experimental exposure. Gray bars encompass the hypothetical in situ irradiance at: the water subsurface; the bottom of the mixed layer; and the mixed layer depth (MLD) average, resulting from applying the subsurface irradiance recorded during the experiment to the in situ mixing conditions. The symbols represent experimental exposure to each band: (A) UVB, (B) UVA, and (C) PAR. 1000 μmol photons m^{-2} s^{-1} approximately equal 220 W m^{-2}.

where the photochemical action spectrum is

$$\varepsilon_{\text{photo},\lambda} = a_{\text{CDOM},\lambda}\phi_\lambda \quad (3)$$

Biological weighting functions (BWFs): Three BWFs, representative of different biological processes, were applied to the average spectral irradiance recorded during whole water incubations (Fig. 2C): one for DNA damage, which is strongly UVB-shifted ($\varepsilon_{\text{SetlowDNA}}$; Setlow 1974); one for phytoplankton DMS release, estimated from a

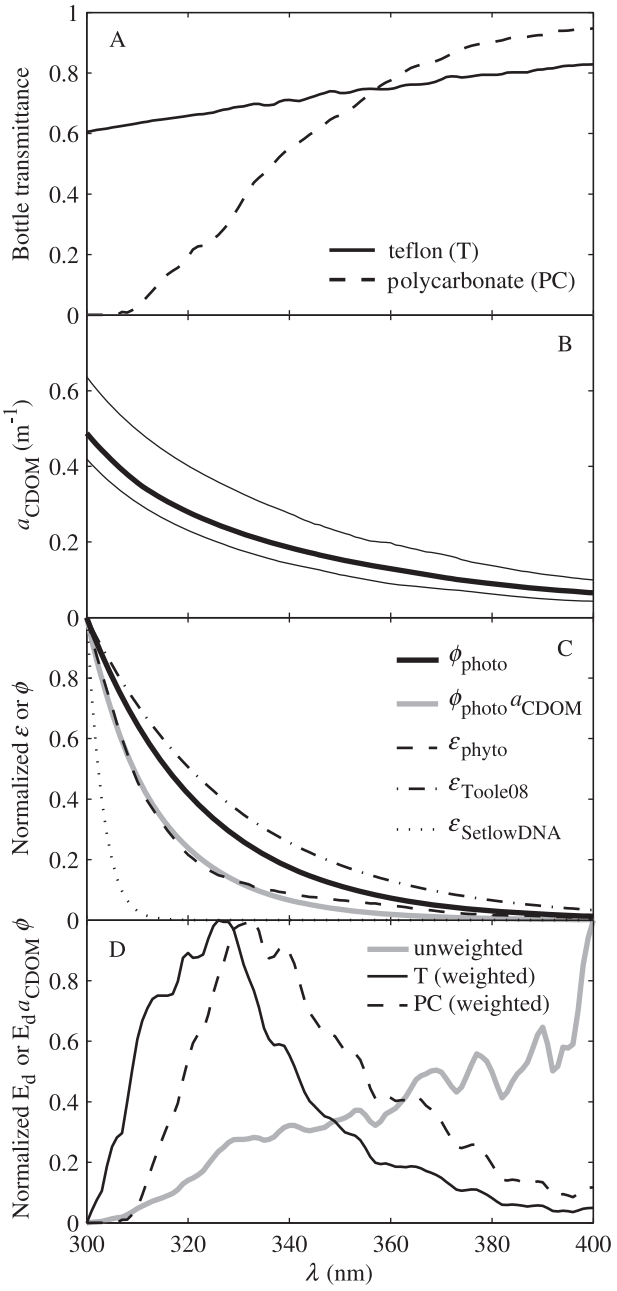

Fig. 2. Graphical example of how biologically or photochemically weighted irradiance was calculated. (A) Spectral transmittance of Teflon and polycarbonate bottles; (B) absorption coefficient of colored dissolved organic matter (a_{CDOM}), with the median of the eight experiments, maximum (26 May 2009) and minimum (30 September 2008); (C) average spectral quantum yield (ϕ_{photo}) and action spectrum ($\phi_{photo} a_{CDOM}$) of DMS photolysis, compared to an average BWF for the inhibition of photosynthesis (ε_{phyto}), a proposed BWF for UV-induced DMS production by phytoplankton ($\varepsilon_{Toole08}$), and a BWF for DNA damage ($\varepsilon_{SetlowDNA}$) (BWFs defined in the text); (D) comparison of the spectral shape of DMS photolysis in Teflon and PC bottles, and unweighted UV irradiance. (C, D) The spectra are normalized to their maximum between 300 and 400 nm.

diagnostic modeling study in the Sargasso Sea, with an exponential spectral slope of 0.0340 nm^{-1} that results in UVA-shifted weights ($\varepsilon_{Toole08}$; Toole et al. 2008); and a BWF representative of photosynthesis photoinhibition, with intermediate UVB vs. UVA weights (ε_{phyto}). Most published BWFs for photosynthesis are biased towards large-celled phytoplankton, which are rarely dominant at the BBMO (Gutiérrez-Rodríguez et al. 2011). Therefore, the average BWF for natural plankton assemblages calculated by Neale and Kieber (2000) was further averaged with the BWF calculated for two picoplankters (Sobrino et al. 2005), which are expected to be more sensitive to UVR (Garcia-Pichel 1994). Fig. 2 is a graphical summary of the optical calculations pipeline, starting with spectral irradiance entering the bottles and ending with wavelength-resolved spectra for each process and treatment.

Sulfur cycling rates—The DMS photolysis rate constant in filtered water incubations (k^*_{photo}) was calculated assuming pseudo first-order kinetics with respect to the weighted irradiance dose (H^*) (Kieber et al. 2007) as follows: First, the natural logarithm of fractional DMS loss in the different irradiance treatments was calculated as $\ln(DMS_0/DMS_f)$, where DMS_0 and DMS_f represent initial and final DMS concentrations, respectively; then, $\ln(DMS_0/DMS_f)$ was regressed against the weighted irradiance dose (H^*). Since the latter accounts for variations in both incubation time and spectral conditions, a linear relationship between the two variables is expected, and k^*_{photo} is the slope of the regression. The units of k^*_{photo} calculated in such a manner are those of $(H^*)^{-1}$.

Net DMS production rate (NP) in unfiltered water incubations was calculated as the change in DMS between the beginning and the end of the incubation (nmol L^{-1} h^{-1}). Since NP results from the balance between biological and photochemical processes, it has to be corrected by the photochemical DMS consumption (PH_{bio}) to obtain the net biological DMS production: $NP_{bio} = NP + PH_{bio}$. At any time, the photolysis rate (PH_{bio}) in whole water bottles can be calculated as the product of k^*_{photo}, weighted irradiance E^*_{bio}, and DMS concentration. Estimating the average photolysis rate would require measuring DMS with sufficient temporal resolution. Since only initial and final DMS were measured, we assumed that the mean photolysis rate in each incubation was proportional to the average E^* and DMS concentration:

$$PH_{bio} = k^*_{photo} E^*_{bio} \overline{DMS}_{bio} \quad (4)$$

Finally, gross DMS production rates (GP) were calculated by budgeting as

$$GP = NP + PH_{bio} + BC \quad (5)$$

where BC stands for bacterial DMS consumption. To estimate dark bacterial DMS consumption (BC_{dark}), one of the two dark bottles (2.9 liters, amber glass) was amended before the incubation with 200–300 nmol L^{-1} dimethyldisulfide (DMDS), an effective inhibitor of bacterial DMS consumption (Wolfe and Kiene 1993; Simó et al. 2000). The difference between DMS production rates in the

DMDS-amended and the unamended bottle yielded $BC_{dark} = GP_{dark} - NP_{dark}$. Field studies using radioisotope additions have shown that solar radiation inhibits DMS consumption, roughly, as much as bacterial leucine incorporation (Toole et al. 2006; Kieber et al. 2007). Thus, in sunlit incubations, BC rates were calculated as the product of BC_{dark} and the fractional inhibition of bulk bacterial leucine incorporation rates (I_{LIR}), as $BC = BC_{dark} \times I_{LIR}$. We took this alternative approach based on bulk bacterial heterotrophic activity photoinhibition because our study, unfortunately, began before the DMDS inhibition had been optimized for its use in light incubations (Galí et al. 2011).

Sources of uncertainty—To estimate the uncertainty associated to budget-derived GP (Eq. 5), the error in each individual measurement was propagated following standard methods (Taylor 1997). We considered the uncertainty in BC and NP rates due to analytical error and incubation duplicates (when existing), and the error of photolysis (Table 3). Error was defined as the range, in the case of duplicates, or as the standard error, when triplicates or more measurements existed.

Besides the measurement error, some uncertainty in GP arose from the assumptions made in its calculation. The first assumption was that BC was photoinhibited to the same extent as microbial leucine incorporation. To address this issue we conducted sensitivity tests where two extreme scenarios were considered: no photoinhibition of BC in sunlight, and total photoinhibition of BC in the harshest exposure (T bottles). According to published data, both extreme assumptions are unlikely to happen (Toole et al. 2006; Kieber et al. 2007). These exercises showed that calculating BC in alternative ways would have little effect on GP rates, and that the change would be generally smaller than the measurement uncertainty.

The second assumption implied that DMS photolysis was proportional to the average of initial and final DMS concentration (Eq. 4). This issue was addressed by calculating a time-resolved photolysis using the recorded irradiance time series. Such calculation was repeated with different patterns of temporal DMS evolution during the incubation. This exercise showed that the bias in the photolysis term (PH_{bio}) derived from the simplification used in Eq. 4 was $< 10\%$, and that DMS evolution could not have departed too much from linearity in most incubations (as already described in Galí et al. 2011). This is in line with DMS measurements performed at an intermediate time in SU1 (1.5 h after solar noon), which indicated almost linear DMS evolution.

Results

Initial microbial communities—Phytoplankton biomass and community composition ranged from high-biomass, diatom-dominated communities in late winter (WI1) to low-biomass, picoplankton-dominated communities in late summer and early autumn (SU1–3, AU1). Spring samples showed an intermediate position and were dominated by nanoflagellates (Table 1; Fig. 3A). Regarding bacterial communities, the SAR 11 clade numerically dominated almost all year-round, with higher abundance in late summer and early autumn, whereas the *Gammaproteobacteria*, *Bacteroidetes*, and *Roseobacter* clades were relatively more abundant during spring (Fig. 3B).

Phytoplankton activity and response to sunlight—Maximum, uninhibited PPp rates occurred in WI1 and SP3 samples ($\sim$ 120 nmol C L^{-1} h^{-1}) and minimum in SU1–3 and AU1 (37–56 nmol C L^{-1} h^{-1}), with intermediate values in SP1–2 (64–79 nmol C L^{-1} h^{-1}). The photoacclimation parameter ($E_k = P^b_{max}/\alpha$) varied between 294 and 2280 μmol photons m^{-2} s^{-1} (median of 537), and showed no obvious relation to light levels in the field. The values of E_k indicate that, in the non-dimmed treatments, the samples spent most of the time on the PAR-saturated portion of the photosynthesis–irradiance curve. Initial $F_v : F_m$ values varied in a narrow range (0.48–0.61), indicative of good physiological condition. At the end of the experiments only slight inhibition was observed, $F_v : F_m$ being reduced to 85.9 $\pm$ 1.8% (T), 87.6 $\pm$ 2.0% (PC), 87.1 $\pm$ 2.0% (T_{dim}), and 91.6 $\pm$ 3.4% (PC_{dim}) of its initial values (average $\pm$ SE, $n = 5$).

In WI1 and SU1–3, subsamples for $F_v : F_m$ were taken at 2–4 intermediate times during the incubation. During the first hour of exposure, $F_v : F_m$ decreased to 38–73% of its initial value in T bottles. By the time peak irradiance was reached, $F_v : F_m$ levels had recovered substantially (Fig. 4), even in bottles suffering the harshest exposure. Thus, the initial photoinhibition (or even "light shock") was reversible, and phytoplankton (as a bulk) were able to photoacclimate. Note that at the time when incubations started (3 h before solar noon), irradiance was on average 40% and 60% of the noontime maximum for the 305 nm and PAR bands, respectively.

Bacterial activity and response to sunlight—Bulk bacterial heterotrophic activity, as indicated by initial leucine (leu) incorporation rates (LIR), was highest in SP2 and SU1 (74–84 pmol leu L^{-1} h^{-1}), and lowest in WI1 (10 pmol leu L^{-1} h^{-1}), with intermediate values in the remaining samples (18–52 pmol leu L^{-1} h^{-1}). Solar exposure generally inhibited leucine incorporation but, on occasion, slight stimulation was also observed (mostly in PC_{dim} bottles). Overall, sunlight incubations yielded LIR values (average $\pm$ SE, $n = 6$) that were 73.3% $\pm$ 6.1% (T), 88.6% $\pm$ 7.3% (PC), 93.0% $\pm$ 8.3% (T_{dim}), and 106.9% $\pm$ 8.5% (PC_{dim}) those of dark incubations. In SP3 and SU2 experiments, where no postexposure LIR measurements were available, the average of the other experiments was used to calculate the inhibition of bacterial DMS consumption.

DMS photolysis—Maximum photolysis rates occurred in T bottles, followed by PC or T_{dim}, and PC_{dim}. In each experiment, the logarithm of fractional DMS loss showed a linear relationship with weighted irradiance dose (H^*). The R^2 of the regression was 0.89–0.99 (except in SU1, $R^2 = 0.83$ with $n = 3$) and the slope significantly different from 0 (Table 3). The intercepts of the regression were never significantly different from 0, as expected, since no photolysis occurs in the dark. For this reason, k^*_{photo} was deduced from the slope

Table 3. Relationship between change in DMS concentration and the weighted irradiance dose (H*) in incubations of filtered (photochemistry) and unfiltered seawater (biological processes). Variables known to affect DMS photolysis are also included: The absorption coefficient of colored dissolved organic matter (a_{CDOM}) and its spectral slope (S_{CDOM}), and nitrate + nitrite concentration. k^*_{photo} is the slope (± standard error, $n = 3$ to 5) of the linear least squares regression between the logarithm of fractional DMS loss and H*. An analogous k has been calculated for unfiltered water incubations ("$k^*_{unfiltered}$", $n = 5$ except in SP3 where $n = 3$). The Y-intercept of the regression ($Y_{x=0}$) is reported for unfiltered water incubations only (*see* text); p values indicate the probability that the slope (k) is different from 0; na, not available.

	Photolysis incubations (0.22 μm filtered water)					Biological process incubations (unfiltered)		
Experiment	$a_{CDOM,300}$ (m^{-1})	S_{CDOM} (nm^{-1})	$NO_{3-}^- + NO_2^-$ μmol L^{-1}	$k^*_{photo} \pm SE$	p	$k^*_{unfiltered} \pm SE$	$Y_{x=0} \pm SE$	p
WI1	0.48	0.020	4.6	−27.7±1.3	0.001	2.4±16.9	−0.02±0.10	0.90
SP1	0.52	0.018	0.12	−23.8±1.3	0.01	−0.9±7.8	0.56±0.08	0.91
SP2	0.61	0.018	0.09	−16.4±0.9	0.009	−9.7±1.2	0.58±0.02	0.004
SP3	0.50	0.017	0.13	na	na	0.4±2.5	0.06±0.04	0.90
SU1	0.48	0.021	0.21	−14.4±1.1	0.11	−3.5±1.2	0.26±0.02	0.06
SU2	0.47	0.020	0.02	−18.7±2.4	0.007	−1.7±2.1	−0.03±0.04	0.48
SU3	0.50	0.022	0.64	−15.9±0.6	0.001	−0.8±1.7	−0.09±0.03	0.66
AU1	0.42	0.019	0.26	−7.1±0.2	0.01	−18.7±9.5	0.1±0.05	0.14

of the regression forced through 0. These observations indicate that DMS photolysis was well described by pseudo first-order kinetics, and that the spectral weighting functions used were appropriate because they accounted for the spectral variation between T and PC bottles.

Photolysis "yields" (k^*_{photo}) decreased by 4-fold from late winter through early autumn (Table 3). In fact, k^*_{photo} was significantly correlated to the day of the year (Spearman's rank correlation $r = -0.93$, $p < 0.01$). The highest photochemical yield occurred in WI1, coinciding with relatively high nitrate concentration (Table 3), in keeping with previous findings (Bouillon and Miller 2004). Besides the variation in photolysis yields, maximum DMS photolysis rates (T bottles) were largely driven by irradiance and DMS concentration (Eq. 4). Thus, highest photolysis rates occurred in SP2 and SU1 (0.54–0.60 nmol L h^{-1}), intermediate values in the rest of summer and spring experiments (0.21–0.36 nmol L h^{-1}), and lowest values in WI1 (0.14 nmol L h^{-1}) and AU1 (0.02 nmol L h^{-1}). Photolysis rates averaged over the duration of each incubation are represented in Fig. 5.

Net DMS production—The highest NP occurred in SP1, SP2, and SU1 experiments, with 0.21–0.46, 0.43–0.53, and 0.21–0.31 nmol L^{-1} h^{-1}, respectively. All other experiments yielded lower NP rates between −0.06 and 0.05 nmol L^{-1} h^{-1}. More interestingly, NP rates displayed a rather flat response across the different treatments (Fig. 5A–H). The slope of the regression between NP and radiation dose was never significantly different from 0, no matter whether the radiation dose was expressed as a specific band (UVB, UVA, PAR) or weighted by any of the spectral weighting functions ($p > 0.2$). In other words: across the spectral irradiance gradient, biological DMS production increased enough to (at least) compensate photochemical DMS loss. The only exception to this behavior was found in AU1 (although the low DMS concentrations and cycling rates in that experiment might have rendered noisier estimations). To provide additional evidence for this finding, we made the exercise of regressing the logarithm of fractional DMS change in unfiltered water incubations to the photolysis-weighted irradiance dose, as done for the photolysis bottles. This clearly showed that, in biological process bottles, DMS evolution departed from the kinetics dictated by DMS photolysis (Table 3).

The lack of treatment replicates in biological process bottles in the first five experiments might limit the strength of our conclusions. However, there are indications that the behavior we observed was robust: (1) the flat response of NP across the spectral irradiance gradient was found in several independent samples; (2) similar NP and photolysis k's were found in experiments performed with similar initial samples, i.e., on sampling dates that were close in time (SP1 vs. SP2, and SU2 vs. SU3); and (3) in the three experiments where biological process bottles were duplicated (SU2–3 and WI1) the error between duplicates was as small as the analytical error (< 5%), which indicates that the large incubation volumes (2.3 liters) minimized artifacts by ensuring community-inclusive incubations (Galí et al. 2011).

Bacterial DMS consumption—Dark BC rates were highest in SP1 and SP2 (0.33 ± 0.15 and 0.11 ± 0.08 nmol L^{-1} h^{-1}, respectively) and lower in the other experiments (between 0.04 and 0.09 nmol L^{-1} h^{-1}), being virtually undetectable in SU1 (0.02 ± 0.03 nmol L^{-1} h^{-1}). BC rate constants, that is, BC rates normalized to the initial DMS (BC/DMS_0; d^{-1} units) were very similar to those found by Vila-Costa et al. (2008) both in magnitude and in terms of seasonal variation. The highest values were found in spring (around 1 d^{-1}) and the lowest in summer (around 0.3 d^{-1}). Only the WI1 sample, with 0.04 ± 0.01 nmol L^{-1} h^{-1} (0.3 d^{-1}), deviated from the general wintertime behavior (1.0 ± 0.4 d^{-1}) found by Vila-Costa et al. (2008).

Net biological and gross DMS production—NP_{bio} displayed a strong response to spectral irradiance. This resulted from adding irradiance-dependent photolysis rates to NP rates that were comparatively smaller and flat across the spectral irradiance gradient (Fig. 5A–H). In all experiments but one (AU1), highest NP_{bio} occurred in the T bottles,

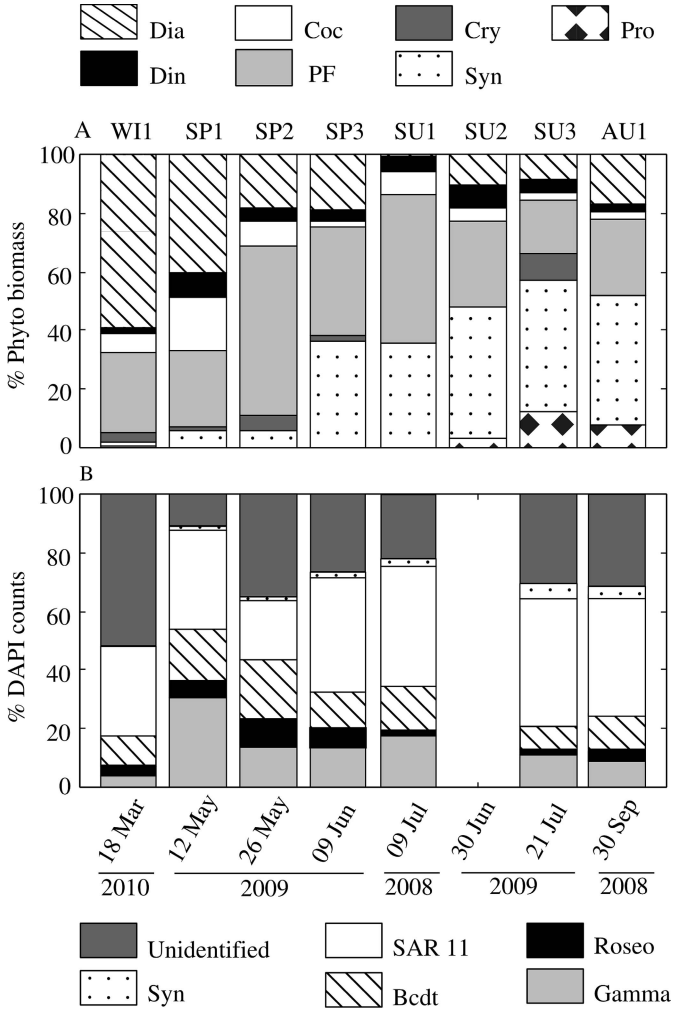

Fig. 3. (A) Contribution of different groups to total phytoplankton carbon biomass, as assessed by flow cytometry and microscopy. Dia, diatoms (*Bacillariophyceae*); Din, dinoflagellates (*Dinophyceae*); Cry, *Cryptophyceae*; Syn, *Synechococcus*; Coc, coccolithophorids (*Prymnesiophyceae*); PF 2–5 μm, phototrophic nanoflagellates; Pro, *Prochlorococcus*. According to Gutiérrez-Rodríguez et al. (2011), the phototrophic nanoflagellates fraction (PF) contains high proportions of small prymnesiophytes, but also pelagophytes and, in winter, prasinophytes. (B) Contribution of different groups to total bacterial numbers, as assessed by CARD-FISH. No data were available for SU2 (30 June 2009). However, other variables indicated that that sampling took place during a smooth transition between late-spring and midsummer conditions. Unidentified, unlabeled prokaryotes; Syn, *Synechococcus*; SAR 11 (*Alphaproteobacteria*); Bcdt, *Bacteroidetes*; Roseo, *Roseobacter* (*Alphaproteobacteria*); Gamma, *Gammaproteobacteria*.

followed by PC or T_{dim}. Samples exposed to mild irradiance (PC_{dim}) showed NP_{bio} rates very similar to those incubated in the dark. Gross DMS production (GP) rates, calculated as the sum of BC and NP_{bio} (Eq. 5), showed a pattern very similar to that of NP_{bio} (Fig. 5A–H). Maximum GP rates in T bottles were found in SP1–2 and SU1 (0.84–1.07 nmol L^{-1} h^{-1}) followed by the remaining samples (0.22–0.46 nmol L^{-1} h^{-1}) and AU1 (< 0.05 nmol L^{-1} h^{-1}). Interestingly, the degree of GP stimulation by sunlight was highly variable despite the qualitatively consistent response (Fig. 6).

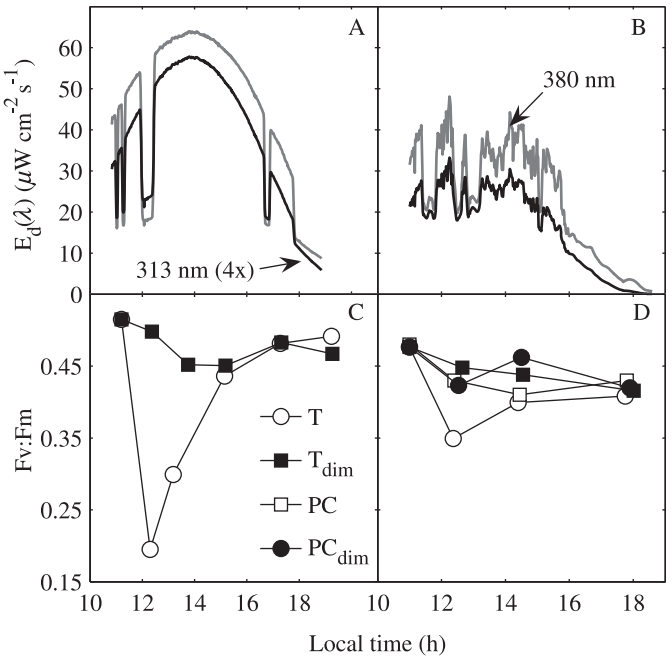

Fig. 4. (A, B) Time series of spectral irradiance at two representative wavebands centered at 313 nm (UVB) and 380 nm (UVA), and (C, D) corresponding time courses of phytoplankton photoinhibition. The examples correspond to two days with different solar zenith angle and cloudiness: (A, C) SU3 and (B, D) WI1.

Sources of uncertainty—Our GP estimates had an average uncertainty of 24%, and the error was $< 33\%$ in 80% of the incubations ($n = 38$). The relative contribution of NP, photolysis (PH_{bio}), and BC to GP varied for each initial sample and treatment (Fig. 5). GP became more sensitive to the PH_{bio} term as spectral irradiance increased, while the importance of BC decreased. Across treatments, the error of PH_{bio} contributed on average 59%, 52%, 31%, and 14% of the GP error in T, PC, T_{dim}, and PC_{dim}, respectively. BC contributed 30%, 31%, 39%, 61%, and 78% in T, PC, T_{dim}, and PC_{dim}, and the dark treatment, respectively. The remaining 11–30% of the error was due to NP.

Discussion

Short-term modulation of community gross DMS production by meteorological forcing has been in the spotlight since the studies of Simó and Pedrós-Alió (1999*a*,*b*). These studies pointed out that photobiological processes mediated by vertical mixing could result in enhanced DMS yields. Indeed, our results show that gross DMS production (GP) can increase dramatically under full-spectrum midday irradiance. Yet, the strength and spectral behavior of the stimulation response are highly variable (Figs. 5, 6). In the following paragraphs we will discuss how this variability can be understood by analyzing the response of GP to spectral irradiance, and its relationship with the structure of the microbial community and its light-exposure history.

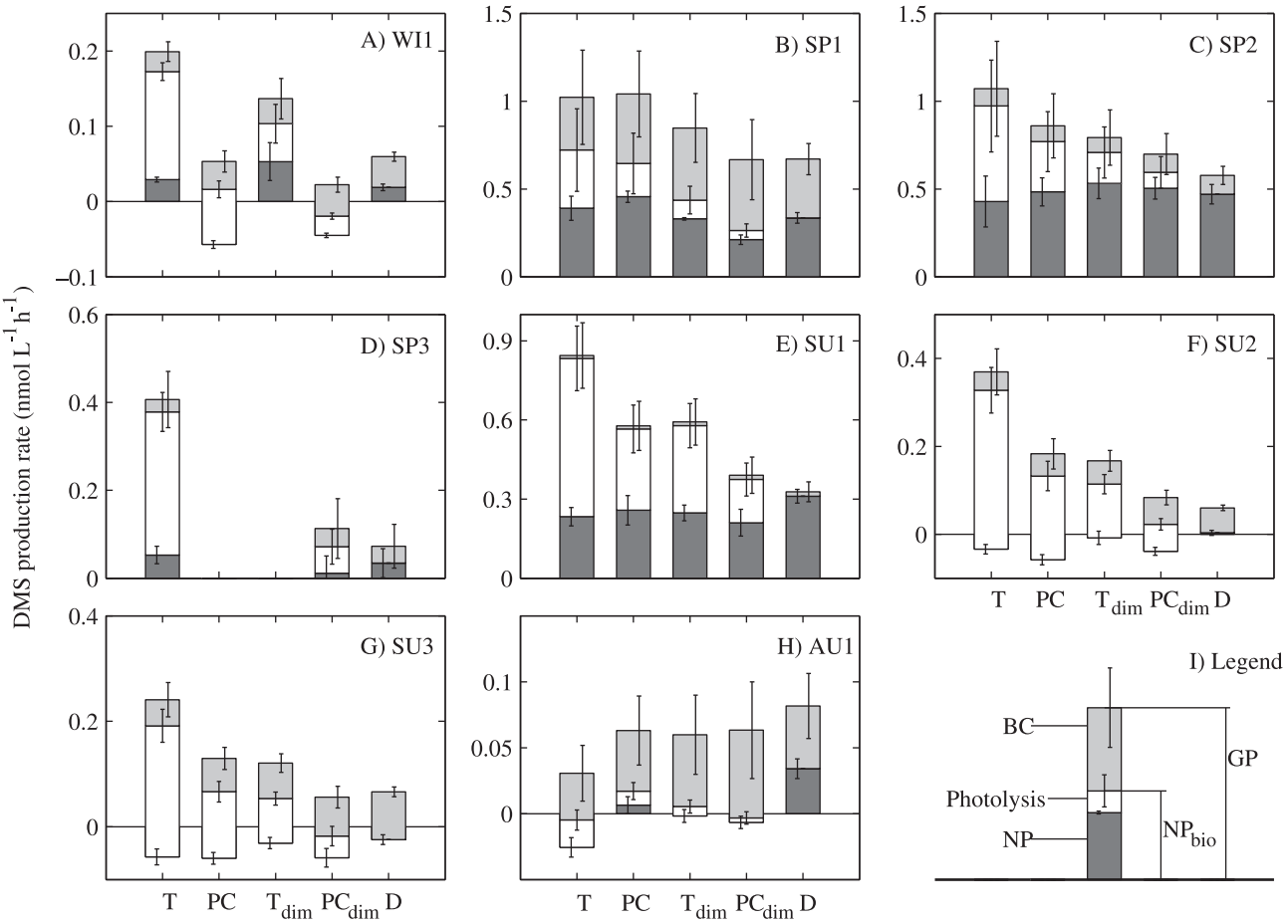

Fig. 5. (A–H) Gross DMS production (GP) rates in the eight experiments, and the contribution of each budget term used for its calculation, namely: net DMS production (NP), DMS photolysis, and bacterial DMS consumption (BC). Net biological DMS production (NP_{bio}) is NP + photolysis. (I) Sketch showing how to interpret the color coding of the bars.

Irradiance dependence of gross DMS production (GP)—The clearest outcome of our experiments is that sunlight-stimulated GP is irradiance dependent. As shown in Fig. 5, the increase in GP across the spectral irradiance gradient is balanced by photolysis, producing the observed flat response of net DMS production (NP). Such response had been already reported by Toole et al. (2006; *see* fig. 9 of that paper), who envisioned the occurrence of radiation-driven GP but did not explore in detail the magnitude and photobiological basis of this process. Our GP stimulation estimate is clearly higher than the 1.3–1.8 range of the stimulation factor reported by Galí et al. (2011). In that study the samples were incubated during 24–29 h, spending less of the total incubation time at high irradiance. This suggests that highest GP occurs during the hours of harshest UVR-PAR exposure, and that the stimulation effect becomes relatively less important on a daily basis.

The lack of short-term effects of UVR on net DMS production contrasts with the strong seasonal relationship between UVR and DMS seasonality (Toole and Siegel 2004). This apparent paradox can be understood by the superposition of the short-term processes analyzed here and the seasonal succession of plankton communities towards enhanced DMS(P) dynamics in summer (Vila-Costa et al. 2008). In this context, sunlight-driven GP can provide the DMS surplus that compensates for photolysis in highly irradiated and stratified waters. This fits with the observation of no DMS depletion (or even net DMS increase) around noontime in studies where surface DMS was measured across diel cycles in summer (Gabric et al. 2008; Galí et al. unpubl.).

It is worth mentioning that the GP rates derived from our experimental design are incubation averages, which result from integrating dose-dependent nonlinear photolysis over time. At this stage, it is unclear whether GP rates are a function of the instantaneous photon flux (irradiance), of the cumulative UVR dose, or (most probably) of both. Work is underway to better comprehend the kinetics of sunlight-dependent gross DMS production, and their dynamic relationship with vertical mixing (Neale et al. 2003).

GP and microbial community structure—The subset of samples exhibiting high NP and GP rates (SP1–2 and SU1) shared a number of characteristics, in some cases significantly different from the remaining samples (two-group Kruskal–Wallis test; $n = 8$; df = 1): elevated DMSPt concentrations ($p < 0.05$); high proportions of DMSP producers ($p < 0.05$), as deduced from the sum of

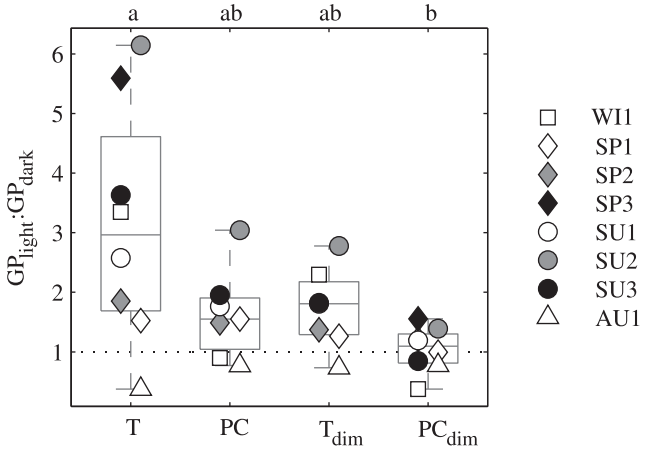

Fig. 6. Stimulation factor of gross DMS production (GP) in sunlit vs. dark incubations in each experiment. The boxes encompass the first and third quartiles, with center in the median. Differences between treatments were significant in the ensemble of all experiments (Kruskal–Wallis $p < 0.05$), as deduced from multiple comparisons (post hoc Tukey–Kramer test; indicated by different letters).

coccolithophores, dinoflagellates, and non-prasinophyte nanoflagellates (most of which were probably prymnesiophytes; Gutiérrez-Rodríguez et al. 2011); and high proportions of bacterial clades putatively harboring DMSP cleavers (Curson et al. 2011), such as *Gammaproteobacteria* (specifically its subclade NOR5, $p < 0.05$), or *Roseobacter* (highest in SP1–3 but not in SU1). The *Bacteroidetes* clade was also more abundant in the SP1–2 and SU1 samples ($p < 0.05$). Another interesting feature was the significant correlation between DMSPt and leucine incorporation rate (Spearman's $r = 0.88$, $p < 0.01$). In summary, we could identify phyto- and bacterioplankton communities that were geared towards high DMS production, concurrent with high bacterial activity, possibly associated to active DMSP catabolism. However, elevated DMS production (SP1–2, SU1) did not co-occur with the strongest stimulation (SP3, SU2–3, and WI1), suggesting that the response to light was not determined by community structure.

Spectral response of GP—In our experimental approach GP responded, by definition, to irradiance weighted by the spectral shape of DMS photolysis (E^*). Therefore, we wanted to explore whether giving greater weights to other regions of the UVR spectrum would render better or worse prediction of GP rates by E^*. For that purpose we calculated, experiment by experiment, the correlation coefficients between GP and irradiance, weighted by the different spectral weighting functions (Fig. 2), or restricted to specific bands (UVB, UVA, and PAR). Although we found substantial variability in the regions of the spectrum eliciting the strongest response, most experiments represented an average situation where wavelengths in the 320–340 nm band were the best predictors of radiation-dependent GP (Fig. 7A). This region coincides with the spectral peak of photosynthesis photoinhibition (which results from multiplying the action spectrum of photosynthesis inhibition and downwelling irradiance). This apparently surprising result stems from the fact that the action spectra of DMS photolysis and photosynthesis inhibition have remarkably similar shapes (Fig. 2C), and clearly points to phytoplankton as key players in sunlight-stimulated GP. Remarkably, Levine et al. (2012) recently reached a similar conclusion with a totally different approach in a time series study in the Sargasso Sea. They found that potential DMS production by the algal fraction (> 1.2 μm), as deduced from in vitro essays, was associated to the radiation dose at 340 nm in the upper mixed layer.

It can be argued that our results are too heavily influenced by our methodological assumptions. However, in some experiments, the trends encountered in GP were already apparent in net DMS production (NP), before photolysis was accounted for (PH_{bio} term). For example, in WI1, NP was significantly higher in T and T_{dim} than in PC and PC_{dim} (duplicate bottles; Kruskal–Wallis test, $p < 0.05$), indicating that a process specific to the UVB band influenced DMS production (Fig. 5A). As a result, UVB-shifted weighting functions worked best to predict GP rates in that experiment (Fig. 7). In SP1, conversely, NP was similarly high in the T and PC treatments (Fig. 5B,E), suggesting a more important role of UVA and PAR wavelengths. We also observed that, in some experiments, E^* did better at predicting GP than NP_{bio} (Fig. 7B), although the link between NP_{bio} and E^* was methodologically more direct. These results strengthen our view that BWFs are appropriate to parameterize GP.

Due to varying experimental conditions and in situ radiation fields (Fig. 1), the comparison between experiments was not straightforward. For that reason, we took advantage of our experimental design to introduce a responsiveness index (R), defined as the relative increase in GP per unit of relative increase in weighted irradiance:

$$R = \frac{(GP_A - GP_B)/GP_B}{(E^*_A - E^*_B)/E^*_B} \quad (6)$$

The spectral irradiance was weighted using the spectral weighting function of DMS photolysis, and the subscripts A and B represent two hypothetical treatments. Spectral responsiveness (R_{spec}) was calculated from the comparison between T to PC and T_{dim} to PC_{dim} bottles. Analogously, total irradiance responsiveness (R_{tot}) was calculated from the comparison between T to T_{dim} and PC to PC_{dim}.

For a given initial water sample, we found that the responsiveness to a spectral shift was of similar magnitude regardless of whether the T and PC bottles compared had been incubated at high or dimmed irradiance. Similarly, the response to a shift in total irradiance (with the shape of spectrum held constant) was of similar magnitude between treatments, regardless of whether the samples had been incubated in T or PC bottles (Fig. 8A). In other words, GP displayed a consistent response on a weighted irradiance basis. WI1 and SU2–3 exhibited stronger spectral responses ($R_{spec} > R_{tot}$), while SP1–2 showed similar R_{spec} and R_{tot}, and SU1 stronger response to total irradiance ($R_{tot} > R_{spec}$). These exploratory calculations (Figs. 7, 8) suggest that distinct processes, with different

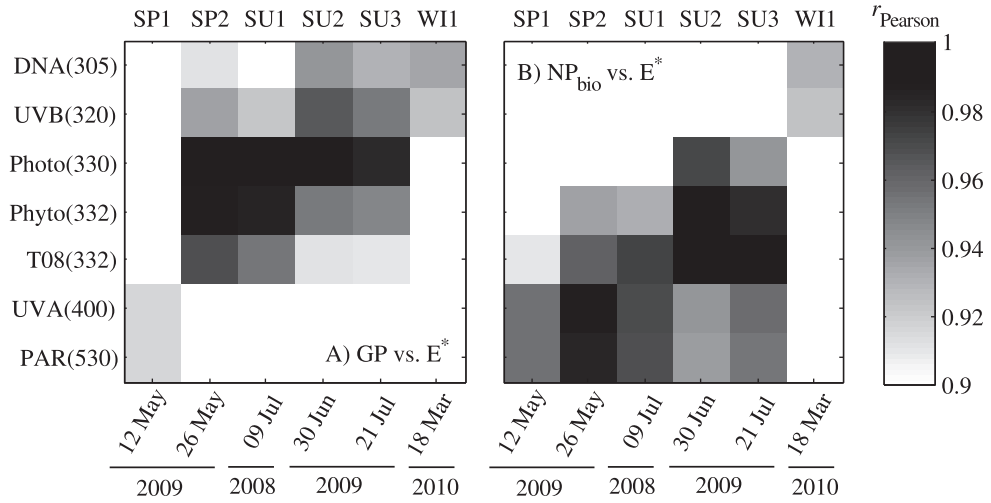

Fig. 7. Graphical representation of the correlation between DMS production in the light treatments and the corresponding irradiance dose ($n = 4$ treatments). (A) Gross DMS production; and (B) net biological DMS production. Irradiance is represented as unweighted wavebands (UVB, UVA, and PAR) or as UV irradiance weighted by different spectral functions (*see* Fig. 2). The weighting functions are sorted from shortwave- to longwave-shifted, and the peak wavelength of each action spectrum is indicated in parentheses. Experiment WI1 has been moved to the end of x-axis for an easier interpretation. Significance levels are $p < 0.01$ for $r > 0.99$, $p < 0.05$ for $r > 0.95$, and $p < 0.1$ for $r > 0.90$; $r < 0.90$ are not included.

spectral sensitivity, might be responsible for the observed stimulation of GP.

Light-exposure history—Although our experimental set-up approximated quite reasonably the in situ irradiance conditions (Fig. 1), we were not equally successful in all the experiments. To assess the relationship between sunlight-stimulated GP and the radiative history of the planktonic community, we calculated an index of experimental overexposure, defined as the quotient between experimental and in situ irradiance for a particular radiation band. The underlying hypothesis was that exposing organisms to irradiances higher than those at which they are acclimated would elicit stronger responses. In congruence with this hypothesis, we found a suggestive relationship between R_{spec} in T bottles and the degree of experimental overexposure to UVB (Fig. 8B) (Spearman's $r = 0.57$, $p = 0.11$; Pearson's $r = 0.70$, $p < 0.05$; $n = 7$). That is, the enhanced response due to inclusion of UVB was somewhat proportional to the degree of experimental overexposure to UVB with respect to the mixed layer average. On the other hand, a less clear relationship was found between R_{tot} and the PAR (or UVA + PAR) overexposure (Spearman's $r = 0.57$, $p = 0.2$; Pearson's $r = 0.52$, $p = 0.23$; $n = 7$).

GP and phytoplankton photophysiology—DMS release may help phytoplankton cells maintain homeostasis at high UVR and PAR, as postulated by the overflow (Stefels 2000) and antioxidant (Sunda et al. 2002) hypotheses. In stratified waters, nutrient depletion can act synergistically with UVR to enhance oxidative stress (Sunda et al. 2007). While not exclusive, these mechanisms should have distinct spectral profiles. Particularly, the antioxidant mechanism should be more responsive to the UV band, which is more effective at generating intracellular radicals (Neale and Kieber 2000).

Extant data suggest that DMS production by phytoplankton can increase by up to one order of magnitude due to UV stress (Sunda et al. 2002; Archer et al. 2010). To explore how feasible was that phytoplankton supplied all the sunlight-stimulated GP (indeed, an extreme supposition), we calculated the amount of primary production channeled through GP. The estimated GP–carbon flux represented a non-negligible fraction of PPp, with a maximum of around 4% (SP1–2 and SU1) and an average ($\pm$ SE) of 1.9 $\pm$ 0.3 ($n = 30$). Furthermore, this fraction was higher in T and T_{dim} bottles than in their PC and PC_{dim} counterparts (by 2-fold, on average; Kruskal–Wallis $p < 0.01$). Considering that phytoplankton can invest as much as 10% of C fixation in DMSP production (Simó et al. 2002; Stefels et al. 2007), the observed GP–carbon flux should be affordable. It is intriguing, however, why such amount of DMS would be released without being oxidized by intracellular radicals to dimethylsulfoxide (DMSO) and further oxidation metabolites. Although we did not measure phytoplankton-derived DMSO production, the possibility exists that some of the intracellular DMSP had been exuded directly as DMSO, as suggested by del Valle et al. (2007), which would imply even higher levels of intracellular DMSP cleavage.

A distinct feature of the antioxidant mechanism would be the upregulation of intracellular DMSP concentrations. In this regard, only a few incubations (WI1, SP1, and SP3; T and/or PC_{dim} bottles) showed a strong increase in

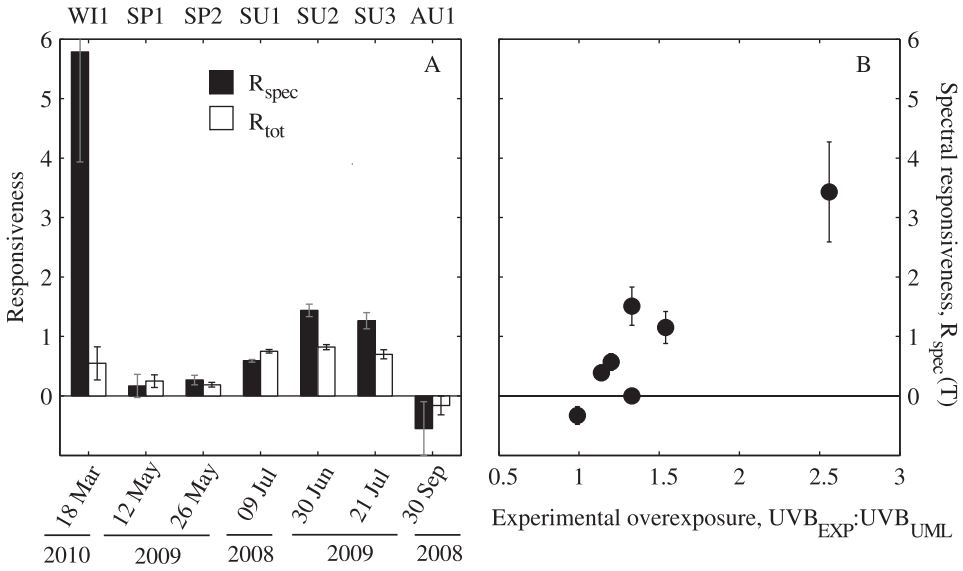

Fig. 8. (A) Comparison between spectral responsiveness (R_{spec}) of gross DMS production vs. its responsiveness to total irradiance (R_{tot}). (B) Relationship between R_{spec} and experimental overexposure to UVB as compared to in situ conditions (*see* text for definitions).

DMSPt concentrations (up to 90%; data not shown). In most incubations we observed slight changes in DMSPt, or even sharp DMSPt decreases (up to −70%), the latter indicating that DMSP synthesis could not keep up with DMSP loss processes.

GP and radiation-induced damage—So far, our results fit in the framework of the overflow and/or antioxidant hypotheses. But if these physiological mechanisms were the predominant response promoting DMS production, why was the largest stimulation observed in SU2–3 and WI1 (Fig. 6), where potential algal DMS producers were not abundant (Fig. 3A)? In our view, an additional mechanism should be considered: radiation-induced phytoplankton cell damage. In this scenario, exposure to sublethal or lethal UVR doses would elicit an increase in the permeability of the cell membrane and, eventually, trigger programmed cell death or necrosis (Bidle and Falkowski 2004). This would make intracellular DMSP available to bacterial, algal extracellular, or dissolved DMS-producing enzymes, resulting in a more accidental (less physiologically regulated) DMS production. This might have been the case in experiments SU2–3, and especially WI1, where the largest stimulation of GP and spectral responsiveness co-occurred with UVB overexposure.

GP and microbial interactions—A long-standing question in DMS cycling studies is resolving the relative importance of the different DMS production pathways. Few studies exist where the influence of grazing and viral lysis on DMS production was determined simultaneously. A culture study carried out by Evans et al. 2007 showed that grazing was more important a DMS production pathway than viruses. Studies done with natural communities demonstrate that grazing-mediated DMS production can represent a dominant pathway for DMS production (Saló et al. 2010). PAR-enhanced grazing and digestion rates in microzooplankton (Strom 2001) may promote DMS production. On the other hand, UVR can worsen the feeding performance of some microzooplankton, alter the nutritional quality of prey, and modify population sizes through trophic cascade effects (Sommaruga 2003). UVB can reduce viral infectivity and, in turn, viral infection can enhance the UVB resistance of some phytoplankton (Jacquet and Bratbak 2003), thereby affecting viral infection–related DMS production. Moreover, UVR can potentially alter DMS-producing microbial interactions at the microscale, which are driven by chemotaxis (Seymour et al. 2010). Altogether, these facts suggest that grazing and viral lysis may play an important (yet uncertain) role in sunlight-stimulated GP, which clearly deserves further investigation. It should also be noted that food web–level effects are probably slower than individual physiological responses, and thus less relevant in our short incubations.

Once algal DMSP has been released by any of the processes discussed above, it can be catabolized by bacteria. We can represent bacterial DMS production as the product of dissolved DMSP concentration (DMSPd; nmol L^{-1}), the rate constant of bacterial DMSPd consumption (dimension $time^{-1}$), and the bacterial DMS yield (%). As irradiance and UVR increase, the rate constant of DMSPd consumption decreases due to photoinhibition (Slezak et al. 2007), and the bacterial DMS yield can either decrease or increase (Slezak et al. 2007; del Valle et al. 2012). Due to these opposed changes, the DMSP cleavage capacity of the bacterial community cannot change dramatically (note that bacterial DMS yields rarely exceed 15%; Kiene and Linn 2000; del Valle et al. 2012). In addition, as UVR and PAR increase,

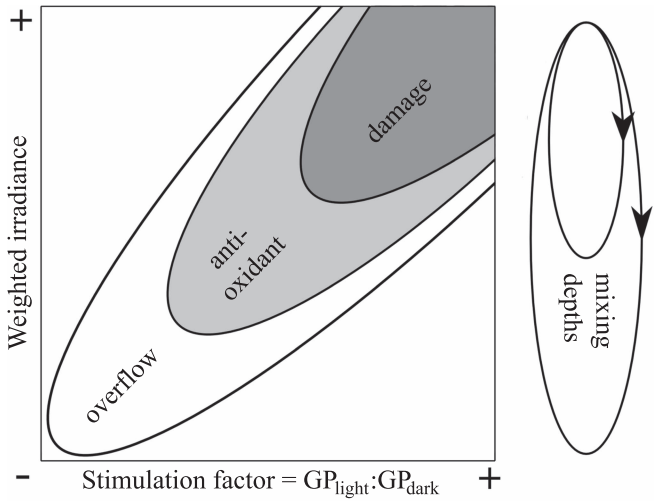

Fig. 9. Conceptual synthesis of the interaction between solar exposure and the stimulation of gross DMS production. The scheme focuses on phytoplankton, since the roles played by bacteria, microzooplankton grazers, and viruses are more uncertain.

DMSP-consuming phytoplankton become more efficient competitors (Ruiz-González et al. 2012*b*). Therefore, bacterial DMS production ultimately relies on the active or accidental release of algal DMSP.

A conceptual framework for sunlight-stimulated GP—The microorganisms thriving in the surface ocean need to be able to cope with changes in the irradiance exposure regime. On one hand, vertical mixing results in a fluctuating irradiance exposure in the turbulent upper layer. On the other hand, diurnal heating and the ensuing stratification can trap a water parcel at the surface, exposing it to continuous high irradiance (our static incubations would resemble the second situation). Due to the spectral dependence of underwater light attenuation, an increase in total irradiance caused by shallow mixing will be accompanied by increasing proportions of shortwave UVR. The dynamic nature of light exposure is still poorly resolved in experimental settings, and its biogeochemical consequences are not well understood (Bertoni et al. 2011; Ross et al. 2011). Our experimental setup, while not totally realistic, provided a first approximation towards understanding the photobiological bases of some DMS production pathways.

In the light of our results, we propose that the overflow and antioxidant mechanisms could be integrated in a wider overflow–antioxidant–damage continuum (Fig. 9), focused on the pivotal role of phytoplankton DMS(P) release. For a given exposure to irradiance, each phytoplankton population will preferentially contribute to DMS production through overflow, antioxidant, or damage mechanisms, depending on its sunlight sensitivity, its constitutive photoprotection strategies, and its DMSP-cleaving capacity. Along a gradient of increasing (weighted) irradiance, the three mechanisms will tend to occur simultaneously, with an increasing importance of damage-related processes and relatively weaker acclimation and repair mechanisms. The interplay between species-specific responses and food-web processes will ultimately determine the variable response of GP to irradiance.

Despite being a coastal site, the BBMO displays rather oceanic characteristics, particularly during the stratification period. For instance, it has salinity levels close to those found in the open Mediterranean (~ 38; Table 1) and microbial plankton assemblages of temperate to subtropical oceans (Gutiérrez-Rodríguez et al. 2011). In correspondence, the concentrations of DMS and its precursor DMSPt are also in the range more frequently found in oceanic waters (Lana et al. 2011). These facts suggest that the photoresponse of GP we observed might be widespread in other oceanic areas displaying seasonal or permanent water column stratification. Indeed, sunlight-stimulated GP has recently been observed in the South Indian subtropical gyre by Galí et al. (2011).

In summary, we have shown that gross DMS production is consistently stimulated by high irradiance and high proportions of shortwave UVR. This highlights the importance of measuring GP under realistic conditions, taking into account that the "light" history of the planktonic community may determine its response to subsequent exposure. Phytoplankton photoinhibition or photodamage are identified as the most likely drivers of sunlight-induced GP. We encourage the use of spectral weighting functions to parameterize sunlight-stimulated GP, always keeping in mind the intricate nature of DMS production by microbial food webs. Our findings provide a process-based understanding of the solar radiation–DMS relationship (Vallina and Simó 2007; Lana et al. 2012), and can help modelers predict DMS concentrations in future scenarios of altered ocean stratification and UV penetration.

Acknowledgments

We thank Ruben Sommaruga and Cristina Sobrino for kindly providing biological weighting functions, the Blanes sampling team for invaluable logistic help, Ramon Massana for the epifluorescence microscopy nanoplankton data, and Cèlia Marrasé for help with microphytoplankton data, colored dissolved organic matter, and useful comments. We are also indebted to Andrés Gutiérrez-Rodríguez, who shared his expertise with the Fast Repetition Rate fluorometer. Two reviewers provided insightful and constructive comments that improved the paper. M.G. acknowledges the receipt of a Junta de Ampliación de Estudios (JAE) scholarship from the Consejo Superior de Investigaciones Científicas (CSIC). This work was supported by the (former) Spanish Ministry of Science and Innovation through the projects "Organic matter sources, microbial diversity, and coastal marine pelagic ecosystem functioning (respiration and carbon use)" (MODIVUS) (Ciencias y Tecnologías Marinas-CTM2005-04795/MAR) and "Surface mixing modulation of the exposure to solar radiation" (SUMMER) (CTM2008-03309/MAR). This is a contribution of the Research Group on Marine Biogeochemistry and Global Change and the Research Group on Aquatic Microbial Food Webs, supported by the Generalitat de Catalunya.

References

Alonso-Sáez, L., and others. 2008. Factors controlling the year-round variability in carbon flux through bacteria in a coastal marine system. Ecosystems **11:** 397–409, doi:10.1007/s10021-008-9129-0

Archer, S. D., M. Ragni, R. Webster, R. L. Airs, and R. J. Geider. 2010. Dimethyl sulfoniopropionate and dimethyl sulfide production in response to photoinhibition in *Emiliania huxleyi*. Limnol. Oceanogr. **55:** 1579–1589, doi:10.4319/lo.2010.55.4.1579

Bertoni, R., W. H. Jeffrey, M. Pujo-Pay, L. Oriol, P. Conan, and F. Joux. 2011. Influence of water mixing on the inhibitory effect of UV radiation on primary and bacterial production in Mediterranean coastal water. Aquat. Sci. **73:** 377–387, doi:10.1007/s00027-011-0185-8

Bidle, K. D., and P. G. Falkowski. 2004. Cell death in planktonic, photosynthetic microorganisms. Nat. Rev. Microbiol. **2:** 643–655, doi:10.1038/nrmicro956

Bouillon, R.-C., and W. L. Miller. 2004. Determination of apparent quantum yield spectra of DMS photodegradation in an in situ iron-induced Northeast Pacific Ocean bloom. Geophys. Res. Lett. **31:** L06310, doi:10.1029/2004GL019536

Charlson, R. J., J. E. Lovelock, M. O. Andreae, and S. G. Warren. 1987. Oceanic phytoplankton, atmospheric sulphur, cloud albedo and climate. Nature **326:** 655–661, doi:10.1038/326655a0

Curson, A. R. J., J. D. Todd, M. J. Sullivan, and A. W. B. Johnston. 2011. Catabolism of dimethylsulphoniopropionate: microorganisms, enzymes and genes. Nat. Rev. Microbiol. **9:** 849–859, doi:10.1038/nrmicro2653

Deal, C., D. J. Kieber, D. A. Toole, K. Stamnes, S. Jiang, and N. Uzuka. 2005. Dimethylsulfide photolysis rates and apparent quantum yields in Bering Sea seawater. Cont. Shelf Res. **25:** 1825–1835, doi:10.1016/j.csr.2005.06.006

del Valle, D. A., D. J. Kieber, J. Bisgrove, and R. P. Kiene. 2007. Light-stimulated production of dissolved DMSO by a particle-associated process in the Ross Sea, Antarctica. Limnol. Oceanogr. **52:** 2456–2466, doi:10.4319/lo.2007.52.6.2456

———, R. P. Kiene, and D. M. Karl. 2012. Effect of visible light on dimethylsulfoniopropionate assimilation and conversion to dimethylsulfide in the North Pacific Subtropical Gyre. Aquat. Microb. Ecol. **66:** 47–62, doi:10.3354/ame01557

Evans, C., S. V. Kadner, L. J. Darroch, W. H. Wilson, P. S. Liss, and G. Malin. 2007. The relative significance of viral lysis and microzooplankton grazing as pathways of dimethylsulfoniopropionate (DMSP) cleavage: An *Emiliania huxleyi* culture study. Limnol. Oceanogr. **52:** 1036–1045, doi:10.4319/lo.2007.52.3.1036

Gabric, A. J, and others. 2008. Factors determining the vertical profile of dimethylsulfide in the Sargasso Sea. Deep-Sea Res. II **55:** 1505–1518, doi:10.1016/j.dsr2.2008.02.002

Galí, M., V. Saló, R. Almeda, A. Calbet, and R. Simó. 2011. Stimulation of gross dimethylsulfide (DMS) production by solar radiation. Geophys. Res. Lett. **38:** L15612, doi:10.1029/2011GL048051

Garcia-Pichel, F. 1994. A model for internal self-shading in planktonic organisms and its implications for the usefulness of ultraviolet sunscreens. Limnol. Oceanogr. **39:** 1704–1717, doi:10.4319/lo.1994.39.7.1704

Gasol, J. M., and P. A. Del Giorgio. 2000. Using flow cytometry for counting natural planktonic bacteria and understanding the structure of planktonic bacterial communities. Sci. Mar. **64:** 197–224, doi:10.3989/scimar.2000.64n2197

Gueymard, C. A., D. Myers, and K. Emery. 2003. Proposed reference irradiance spectra for solar energy systems testing. Sol. Energy **73:** 443–467, doi:10.1016/S0038-092X(03)00005-7

Gutiérrez-Rodríguez, A., M. Latasa, R. Scharek, R. Massana, G. Vila, and J. M. Gasol. 2011. Growth and grazing rate dynamics of major phytoplankton groups in an oligotrophic coastal site. Estuar. Coast. Shelf Sci. **95:** 77–78, doi:10.1016/j.ecss.2011.08.008

Jacquet, S., and G. Bratbak. 2003. Effects of ultraviolet radiation on marine virus-phytoplankton interactions. FEMS Microbiol. Ecol. **44:** 279–289, doi:10.1016/S0168-6496(03)00075-8

Kieber, D. J., D. A. Toole, J. J. Jankowski, R. P. Kiene, G. R. Westby, D. del Valle, and D. Slezak. 2007. Chemical "light meters" for photochemical and photobiological studies. Aquat. Sci. **69:** 360–376, doi:10.1007/s00027-007-0895-0

Kiene, R. P., and L. J. Linn. 2000. The fate of dissolved dimethylsulfoniopropionate (DMSP) in seawater: Tracer studies using ^{35}S-DMSP. Geochim. Cosmochim. Acta **64:** 2797–2810, doi:10.1016/S0016-7037(00)00399-9

Kirchman, D., E. Knees, and R. Hodson. 1985. Leucine incorporation and its potential as a measure of protein-synthesis by bacteria in natural aquatic systems. Appl. Environ. Microbiol. **49:** 599–607.

Lana, A., R. Simó, S. M. Vallina, and J. Dachs. 2012. Re-examination of global emerging patterns of ocean DMS concentration. Biogeochemistry **110:** 173–182, doi:10.1029/CE054p0441

———, and others. 2011. An updated climatology of surface dimethlysulfide concentrations and emission fluxes in the global ocean. Global Biogeochem. Cycles **25:** GB1004, doi:10.1029/2010GB003850

Laney, S. R. 2003. Assessing the error in photosynthetic properties determined with fast repetition rate fluorometry. Limnol. Oceanogr. **48:** 2234–2242, doi:10.4319/lo.2003.48.6.2234

Levine, N. M., V. A Varaljay, D. A. Toole, J. W. H. Dacey, S. C. Doney, and M. A. Moran. 2012. Environmental, biochemical and genetic drivers of DMSP degradation and DMS production in the Sargasso Sea. Environ. Microbiol. **14:** 1210–1223, doi:10.1111/j.1462-2920.2012.02700.x

Marie, D., and F. Partensky. 2006. Analyse de micro-organismes marins, p. 211–233. *In* X. Ronot, D. Grunwald, J.-F. Mayol, and J. Boutonnat [eds.], La cytométrie en flux. Lavoisier. [Analysis of marine microorganisms, *in* Flow cytometry.]

Menden-Deuer, S., and E. J. Lessard. 2000. Carbon to volume relationships for dinoflagellates, diatoms, and other protist plankton. Limnol. Oceanogr. **45:** 569–579, doi:10.4319/lo.2000.45.3.0569

Moran, M. A., C. R. Reisch, R. P. Kiene, and W. B. Whitman. 2012. Genomic insights into bacterial DMSP transformations. Annu. Rev. Mar. Sci. **4:** 523–542, doi:10.1146/annurev-marine-120710-100827

Neale, P. J., E. W. Helbling, and H. E. Zagarese. 2003. Modulation of UVR exposure and effects by vertical mixing and advection, p. 107–136. *In* E. W. Helbling and H. E. Zagarese [eds.], UV effects in aquatic organisms and ecosystems. Comprehensive Series in Photosciences. European Society of Photobiology. Royal Society of Chemistry, London.

———, and D. J. Kieber. 2000. Assessing biological and chemical effects of UV in the marine environment: Spectral weighting functions, p. 61–83. *In* R. E. Hester and R. M. Harrison [eds.], Causes and environmental applications of increased UV-B radiation. Royal Society of Chemistry.

Pernthaler, A., J. Pernthaler, and R. Amann. 2002. Fluorescence in situ hybridization and catalyzed reporter deposition for the identification of marine bacteria. Appl. Environ. Microbiol. **68:** 3094–3101, doi:10.1128/AEM.68.6.3094-3101.2002

Quinn, P. K., and T. S. Bates. 2011. The case against climate regulation via oceanic phytoplankton sulphur emissions. Nature **480:** 51–56, doi:10.1038/nature10580

Romera-Castillo, C., X. A. Álvarez-Salgado, M. Galí, C. Marrasé, and J. M. Gasol. In press. Combined effect of light exposure and microbial activity on distinct dissolved organic matter pools. A seasonal field study in an oligotrophic coastal system (Blanes Bay, NW Mediterranean). Mar. Chem., doi:10.1016/j.marchem.2012.10.004

Ross, O. N., R. J. Geider, and J. Piera. 2011. Modelling the effect of vertical mixing on bottle incubations for determining in situ phytoplankton dynamics. II. Primary production. Mar. Ecol. Prog. Ser. **435:** 33–45.

Ruiz-González, C., T. Lefort, M. Galí, M. M. Sala, R. Sommaruga, R. Simó, and J. M. Gasol. 2012*a*. Seasonal patterns in the sunlight sensitivity of bacterioplankton from Mediterranean surface coastal waters. FEMS Microbiol. Ecol. **79:** 661–674.

———, R. Simó, M. Vila-Costa, R. Sommaruga, and J. M. Gasol. 2012*b*. Sunlight modulates the relative importance of heterotrophic bacteria and picophytoplankton in DMSP-sulphur uptake. ISME J. **6:** 650–659, doi:10.1038/ismej.2011.118

Saló, V., R. Simó, and A. Calbet. 2010. Revisiting the dilution technique to quantify the role of microzooplankton in DMS(P) cycling: Laboratory and field tests. J. Plankton Res. **32:** 1255–1267, doi:10.1093/plankt/fbq041

Setlow, R. B. 1974. The wavelengths in sunlight effective in producing skin cancer: A theoretical analysis. Proc. Natl. Acad. Sci. USA **71:** 3363–3366, doi:10.1073/pnas.71.9.3363

Seymour, J. R., R. Simó, T. Ahmed, and R. Stocker. 2010. Chemoattraction to dimethylsulfoniopropionate throughout the marine microbial food web. Science **329:** 342–345, doi:10.1126/science.1188418

Simó, R. 1998. Trace chromatographic analysis of dimethyl sulfoxide and related methylated sulfur compounds in natural waters. J. Chromatogr. A **807:** 151–164, doi:10.1016/S0021-9673(98)00086-7

———. 2004. From cells to globe: Approaching the dynamics of DMS(P) in the ocean at multiple scales. Can. J. Fish. Aquat. Sci. **61:** 673–684, doi:10.1139/f04-030

———, S. D. Archer, C. Pedrós-Alió, L. Gilpin, and C. E. Stelfox-Widdicombe. 2002. Coupled dynamics of dimethylsulfoniopropionate and dimethylsulfide cycling and the microbial food web in surface waters of the North Atlantic. Limnol. Oceanogr. **47:** 53–61, doi:10.4319/lo.2002.47.1.0053

———, and C. Pedrós-Alió. 1999*a*. Role of vertical mixing in controlling the oceanic production of dimethyl sulphide. Nature **402:** 396–399, doi:10.1038/46516

———, and ———. 1999*b*. Short-term variability in the open ocean cycle of dimethylsulfide. Global Biogeochem. Cycles **13:** 1173–1181, doi:10.1029/1999GB900081

———, ———, G. Malin, and J. O. Grimalt. 2000. Biological turnover of DMS, DMSP and DMSO in contrasting open-sea waters. Mar. Ecol. Prog. Ser. **203:** 1–11, doi:10.3354/meps203001

———, M. Vila-Costa, L. Alonso-Sáez, C. Cardelús, Ò. Guadayol, E. Vázquez-Domínguez, and J. M. Gasol. 2009. Annual DMSP contribution to S and C fluxes through phytoplankton and bacterioplankton in a NW Mediterranean coastal site. Aquat. Microb. Ecol. **57:** 43–55, doi:10.3354/ame01325

Slezak, D., R. P. Kiene, D. A. Toole, R. Simó, and D. J. Kieber. 2007. Effects of solar radiation on the fate of dissolved DMSP and conversion to DMS in seawater. Aquat. Sci. **69:** 377–393, doi:10.1007/s00027-007-0896-z

Smith, D., and F. Azam. 1992. A simple, economical method for measuring bacteria protein synthesis rates in seawater using ^{3}H-leucine. Mar. Microb. Food Webs **6:** 107–114.

Sobrino, C., P. J. Neale, and L. M. Lubián. 2005. Interaction of UV radiation and inorganic carbon supply in the inhibition of photosynthesis: Spectral and temporal responses of two marine picoplankters. Photochem. Photobiol. **81:** 384–393, doi:10.1562/2004-08-27-RA-295.1

Sommaruga, R. 2003. UVR and its effects on species interactions, p. 485–508. *In* E. W. Helbling and H. E. Zagarese [eds.], UV effects in aquatic organisms and ecosystems. Comprehensive Series in Photosciences, European Society of Photobiology. Royal Society of Chemistry, London.

Stefels, J. 2000. Physiological aspects of the production and conversion of DMSP in marine algae and higher plants. J. Sea Res. **43:** 183–197, doi:10.1016/S1385-1101(00)00030-7

———, M. Steinke, S. M. Turner, G. Malin, and S. Belviso. 2007. Environmental constraints on the production and removal of the climatically active gas dimethylsulphide (DMS) and implications for ecosystem modelling. Biogeochemistry **83:** 245–275, doi:10.1007/s10533-007-9091-5

Strom, S. L. 2001. Light-aided digestion, grazing and growth in herbivorous protists. Aquat. Microb. Ecol. **23:** 253–261, doi:10.3354/ame023253

Sunda, W., D. J. Kieber, R. P. Kiene, and S. Huntsman. 2002. An antioxidant function for DMSP and DMS in marine algae. Nature **418:** 317–320, doi:10.1038/nature00851

Sunda, W. G., R. Hardison, R. P. Kiene, E. Bucciarelli, and H. Harada. 2007. The effect of nitrogen limitation on cellular DMSP and DMS release in marine phytoplankton: Climate feedback implications. Aquat. Sci. **69:** 341–351, doi:10.1007/s00027-007-0887-0

Taylor, J. R. 1997. An introduction to error analysis. Univ. Science Books.

Toole, D. A., D. J. Kieber, R. P. Kiene, D. A. Siegel, and N. B. Nelson. 2003. Photolysis and the dimethylsulfide (DMS) summer paradox in the Sargasso Sea. Limnol. Oceanogr. **48:** 1088–1100, doi:10.4319/lo.2003.48.3.1088

———, and D. A Siegel. 2004. Light-driven cycling of dimethylsulfide (DMS) in the Sargasso Sea: Closing the loop. Geophys. Res. Lett. **31:** L09308, doi:10.1029/2004GL019581

———, ———, and S. C. Doney. 2008. A light-driven, one-dimensional dimethylsulfide biogeochemical cycling model for the Sargasso Sea. J. Geophys. Res. **113:** 1–20, doi:10.1029/2007JG000426

———, D. Slezak, R. P. Kiene, D. J. Kieber, and D. A. Siegel. 2006. Effects of solar radiation on dimethylsulfide cycling in the western Atlantic Ocean. Deep-Sea Res. I **53:** 136–153, doi:10.1016/j.dsr.2005.09.003

Vallina, S. M., and R. Simó. 2007. Strong relationship between DMS and the solar radiation dose over the global surface ocean. Science **315:** 506–508, doi:10.1126/science.1133680

Vila-Costa, M., R. P. Kiene, and R. Simó. 2008. Seasonal variability of the dynamics of dimethylated sulfur compounds in a coastal northwest Mediterranean site. Limnol. Oceanogr. **53:** 198–211, doi:10.4319/lo.2008.53.1.0198

———, R. Simó, H. Harada, J. M. Gasol, D. Slezak, and R. P. Kiene. 2006. Dimethylsulfoniopropionate uptake by marine phytoplankton. Science **314:** 652–654, doi:10.1126/science.1131043

Webb, W. L., M. Newton, and D. Starr. 1974. Carbon dioxide exchange of *Alnus rubra*. Oecologia **17:** 281–291, doi:10.1007/BF00345747

Wolfe, G., and R. P. Kiene. 1993. Effects of methylated, organic, and inorganic substrates on microbial consumption of dimethyl sulfide in estuarine waters. Appl. Environ. Microbiol. **59:** 2723–2726.

Zepp, R. G., D. J. Erickson, N. D. Paul, and B. Sulzberger. 2007. Interactive effects of solar UV radiation and climate change on biogeochemical cycling. Photochem. Photobiol. Sci. **6:** 286–300, doi:10.1039/b700021a

Associate editor: Mikhail V. Zubkov

Received: 12 March 2012
Accepted: 22 October 2012
Amended: 20 October 2012